Volume XCII, No. 2, Nov 2022

Proceedings of the Danish Society for Structural Science and Engineering

Published by

Danish Society for Structural Science and Engineering

COPENHAGEN 2022

ISSN 1601-6548 (online)

PROCEEDINGS OF THE DANISH SOCIETY FOR STRUCTURAL SCIENCE AND ENGINEERING
Edited and published by the Danish Society for Structural Science and Engineering
Volume 92, No. 2, 2022.

On the influence of transverse reinforcement type and layout on the shear capacity of thin-webbed concrete beams

Jakob Fisker[1]

Christian Svarre[2]

Toke Rask Frandsen[1]

Lars German Hagsten[3]

Abstract

The theory of plasticity represents an attractive and strong basis for design and assessment of reinforced concrete structures. Either through application of so-called lower bound solutions (static method) or by analysing potential failure mechanisms using the upper bound theorem (kinematic method). The application of plasticity theory inevitable also includes the use of reasonable effectiveness factors, introducing a limitation on the magnitude of the concrete strength to be utilized, the effective concrete strength. Effectiveness factors used in practice have all been determined on the basis of testing and are assumed to account for a range of complex phenomena not included directly in the models.

This paper presents the results of an experimental investigation comprising twelve simply supported thin-webbed T-beams. The aim was to study the influence of the transverse reinforcement type and -layout with respect to the cracking- and deformational behaviour and the shear capacity. To this end the beams were subdivided into four groups with transverse reinforcement type and -layout being the only intended variation between the four groups, all failing in shear. In the paper a thorough presentation of experimental observations will be given. Photogrammetric measurements allowed for a detailed analysis of crack-kinematics in combination with the deformations of the concrete web.

[1] Danish technological Institute, Aarhus
[2] Artelia, Aarhus
[3] Aarhus University, Value Engineering ApS

1. Introduction

The diagonal compression field method for design of reinforced concrete beams was developed mainly during the 1970s and early 1980s; particularly on the basis of research in Denmark and Switzerland[1-3]. The method was implemented in the 1984-version of the Danish code for structural concrete, and has also formed the basis for shear design of reinforced concrete beams in Eurocode in many years.

In relation to the early development extensive testing was naturally performed, for the purpose of comparison with theoretical predictions. Typical of that time, the provided stirrup reinforcement was made from smooth or plain bars of mild steel, with a yield strength in the range of 250-350 MPa; much lower when compared to nowadays[4]. The first estimates on a suitable effectiveness factor, providing an upper limit to the compressive stress to be carried by the concrete, were made on the basis of such tests, and the recommendations are almost identical to the provisions of the Eurocode of today[5,6]. Since then the strength of reinforcement steel has steadily increased, and stirrups made from de-formed or ribbed bars gradually became standard in practice concrete construction. In fact, the use of stirrups made from plain bars of mild steel reinforcement has all but vanished, and the application is de facto prohibited by the current Eurocode.

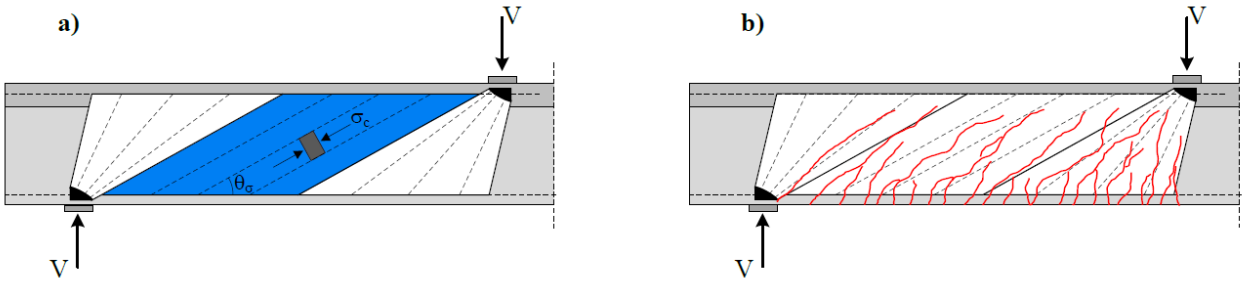

Figure 1: a) *Possible stress field solution with homogeneous state of stress in the intermediate stress field.* ***b)*** *Stress fields with web cracks superimposed*

The inferior properties of plain or smooth bars regarding bond and anchorage are, of course, of great importance when aiming for a safe and durable structure; especially in relation to proper detailing. However, as intuitively reasonable it may appear there is, in many cases, a lack experimental evidence highlighting and quantifying differences in this regard. And when considering shear capacity and the general performance with respect to web-cracking, -stiffness and deformation etc., of beams, the influence of the type and arrangement of the transverse reinforcement is not fully understood. This may lead to challenges when assessing whether an existing concrete structure is fit for further increase of loading and/or changes in load-application.

The focus of the investigation presented in the following has been to study the influence of the transverse reinforcement type and layout on the cracking- and deformational behavior and shear capacity of thin-webbed reinforced concrete T-beams subjected to shear and bending. Specifically, the aim is to identify differences and similarities when considering two different scenarios; stirrups made from plain bars of mild steel and stirrups made from ribbed bars of ordinary strength. To this end, experimental investigations involving twelve tests on T-beams, all failing in shear, and with transverse reinforcement ratios ranging between 0.13% to 0.3%, have been conducted.

Many of the previous tests addressing the shear behavior of reinforced concrete beams have involved large amount of flexural reinforcement, as evidenced by multiple databases on shear tests[7]; perhaps to ensure the desired mode of failure. However, to impose a greater extent of cracking and larger crack widths, the tested beams have been designed so that the flexural capacity only slightly exceeds the expected shear capacity. This gives a better reflection of actual conditions in practice. Also, the effectiveness factor, limiting the concrete compressive stresses, has been shown to be influenced by the extent of cracking and corresponding crack

kinematics. In regard to design, this influence is e.g., manifested by a detrimental influence of an increasing major principal web strain on the size of the effectiveness factor. Such a relation is adopted in certain codes and more recent proposals on shear design[8,9].

In the analysis of the tests, attention is given to the ultimate- and post peak conditions as well as what could be regarded as the serviceability range, where the applied load does not exceed 55-60% of the capacity. In more details, differences and similarities are addressed on the basis of; (1) measured load-displacement relation quantifying potential differences in regards to stiffness and failure-mode ductility or lack hereof, (2) crack patterns in terms of crack density and -spacing, crack directions and changes in crack directions as a function of the applied load, (3) maximum crack widths and distribution of crack widths, and finally (4) crack kinematics and measurements of average web strains including principal directions.

2. Experimental programme

The tests reported in this article were all part of an experimental programme conducted at Aarhus University School of engineering. The programme consisted of twelve specimens, subdivided into four test series.

2.1 Test beams

An overview of the tested beams is given in Figure 2 and Table 1. The specimens were all T-beams with a total length of 5300 mm, subjected to four-point bending, and with a shear span of 1800 mm. All beams had identical cross sections and where provided with a main longitudinal reinforcement consisting of bars 4Ø20+2Ø14, leading to a reinforcement ratio of 1.58% with respect to the total area of the T-section. Besides the main longitudinal reinforcement, two bars Ø10 were placed at mid height of the web according to standard practice for members of this height for crack control.

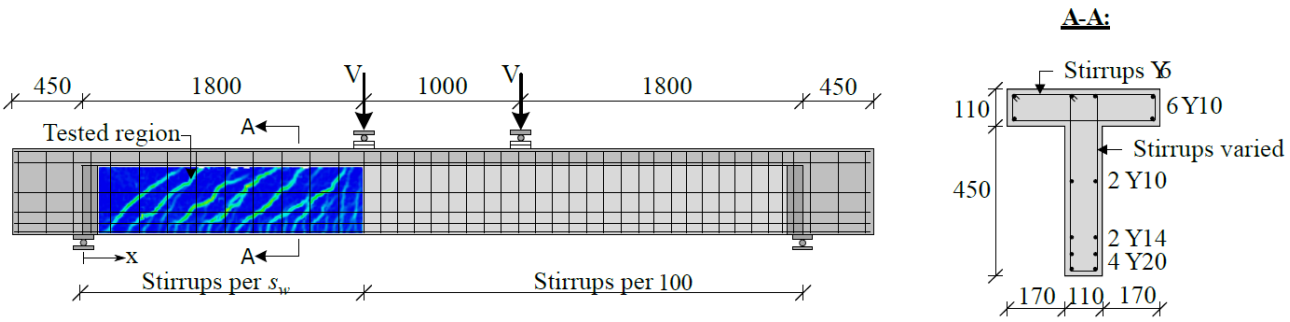

Figure 2: *Test setup and reinforcement layout*

In order to ensure sufficient anchorage and prevent instability issues the web thickness was gradually increased over the length of the support-plates, leaving rectangular cross sections just behind the support.

		S2a	S2b	S2c	R2a	R2b	R2c	S3a	S3b	S3c	R3a	R3b	R3c
f_c	[MPa]	36.0 (1.0)			41.7 (6.4)			37.7 (3.5)			37.2 (3.2)		
d	[mm]	469	475	468	474	485	498	486	473	482	484	482	474
s_w	[mm]	168	174	171	264	272	269	273	264	264	400	400	400
ρ_w	[%]	0.31	0.30	0.30	0.19	0.19	0.19	0.19	0.19	0.19	0.13	0.13	0.13
$f_{t,5}$	[MPa]	1.1	1.1	1.1	1.2	1.1	1.2	0.7	0.7	0.7	0.8	0.8	0.8
profile	-	smooth	smooth	smooth	ribbed	ribbed	ribbed	smooth	smooth	smooth	ribbed	ribbed	ribbed

Table 1: *Properties of tested beams*

2.1.1 Arrangement of transverse reinforcement

The twelve beams were, as mentioned, divided into four groups; R2, R3, S2 and S3; with the type and arrangement of transverse reinforcement being the only intended variation between the groups. For the groups R2 and R3 the transverse reinforcement was made from deformed or ribbed bars Ø6, whereas plain or smooth bars Ø6 where used for groups S2 and S3. Closed two-legged stirrups were used for all beams. The spacing of stirrups, s_w, was chosen under consideration of the equivalent (or "smeared") tensile strength $f_{t,s}$ ($=f_{y,w}/(b_w s_w)$) provided by the stirrups, and so that approximately identical tensile strengths were obtained for groups R2 and S2 and groups R2 and S3, respectively.

To control the location of the shear failure the right-side shear span (see figure 2) was supplied with additional stirrups for all beams. The beams were all cast and cured at a local precast concrete plant. After testing, all reinforcement was uncovered so that the actual location could be determined. Minor variations in the placement of the reinforcement resulted in slight variations of the effective depth and average stirrup spacing.

2.2 Materials

2.2.1 Concrete

Normal strength concrete, with a maximum aggregate size of 16 mm, was used for all beams. Four cylinders (150x300 mm) were cast for each beam. The beam tests were performed over a period of twelve days; one test per day, and each day the compressive strength was measured based on the four cylinders, subjected to uniaxial compression. Table 1 lists the average compressive strength and corresponding standard deviation for each of the four groups of beams.

2.2.2 Reinforcement

Five samples of reinforcement were tested in uniaxial tension for each type of reinforcement used in tests. The obtained strengths (yield- and tensile strength) are listed in Table 2, and stress-strain diagrams for the transverse reinforcement are shown in Figure 3a. Hot-rolled steel was used for the transverse reinforcement in groups S2 and S3 whereas cold-worked steel was used for groups R2 and R3 with deformed bars.

		Ø6 (plain)	Ø6 (ribbed)	Ø10	Ø14	Ø20
f_y / $f_{0.2\%}$	[MPa]	365	602	586	588	604
f_u	[MPa]	566	719	666	674	684

Table 2: *Measured reinforcement properties*

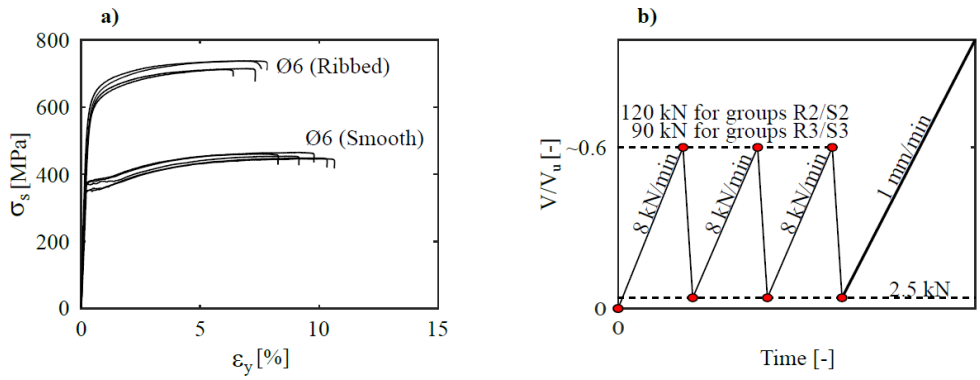

Figure 3*: **a)** stress-strain relations for transverse reinforcement.* ***b)*** *loading procedure*

2.3 Test setup and Instrumentation

Concentrated loads were applied by means of two servo-controlled, hydraulic MTS-actuators. The supports consisted of roller bearings allowing for in-plane horizontal translations and rotations.

Vertical displacements of the upper side of the flange were measured along the tested region using eight linearly variable differential transducers (LVDTs), with the last LVDT placed just next to the left-side actuator. These measurements were later used for validation of photogrammetric measurements.

Photogrammetric measurements were conducted in order to register crack developments and in-plane displacements along the considered shear span. Photogrammetry was performed using the ARAMIS system developed by GOM mbH. During testing, images were captured at a frequency of 1 Hz, and after testing, the photographs were analysed in the software GOM Correlate.

A stochastic pattern of high contrast was achieved by painting the surface of the test specimen with a stochastic black pattern on a white background. Prior to testing of the specimens, different methods of obtaining the required stochastic pattern were investigated. The most reliable and preferred method was to dab black painting onto the white surface using a humid, porous, and soft sponge. Spray paint was used to achieve the white background colour. The quality of the stochastic pattern in combination with the illumination of the tested region was considered acceptable, when pseudo displacements in ARAMIS images of less than 0.05 mm were recorded before any load was applied. The photogrammetric measurements were compared against LVDT measurements and measurements using demountable mechanical strain gauges mounted on the surface of the concrete web. Good agreement was observed. All measurements were collected and synchronized using QuantumX data acquisition units.

2.4 Test procedure

A load of approximately 60% of the expected shear capacity was applied three times before the failure test was commenced (see Figure 3b). During the preliminary load cycles, the load was force-controlled at 8 kN/min. During the failure test, the load was displacement-controlled at 1 mm/min. During the failure test, the displacement measured by the integrated LVDT within the actuator closest to the tested region (left side actuator) served as sensor for the displacement-controlled loading procedure, whereas the right side actuator was force-controlled using the signal from the left-side actuator.

3 Test results and observations

In the following, a selection of various results and observations will be presented. Starting with a brief presentation of overall observations, an analysis highlighting what will be termed the *serviceability behaviour* will be presented in section 3.2. The *ultimate- and post-peak behaviour* is addressed in section 3.3.

3.1 Overall observations

3.1.1 Capacities

All twelve beams failed in an apparent shear failure, and in Table 3 the peak shear force $V_{u,exp}$ and the corresponding displacement $\delta_{peak,exp}$ is listed. The table also includes the ratio between the measured shear capacity and the expected flexural capacity, given by the shear force V_{flex}. The flexural capacity has been estimated using traditional plastic sectional analysis, taking into account the actual materiel parameters and the actual positions of the longitudinal reinforcement. The actual position was determined from removal of the side- and bottom cover after failure of the beams. As seen, the flexural utilization at failure was approximately the same for comparable groups S2 & R2 and S3 & R3, respectively. Finally, the table includes a note concerning the observed mode of shear failure. The designation between failure modes I and II is clarified later.

		S2a	S2b	S2c	R2a	R2b	R2c	S3a	S3b	S3c	R3a	R3b	R3c
$V_{u,test}$	[kN]	190	194	192	200	206	195	158	166	158	177	157	172
mean $V_{u,test}$	[kN]	192.0			203.3			160.7			168.7		
$\delta_{peak,test}$	[mm]	31	30	29	28	29	27	21	23	23	22	21	22
$V_{u,test}$ / V_{flex}	[-]	0.85	0.86	0.87	0.89	0.88	0.83	0.68	0.75	0.69	0.76	0.69	0.76
failure mode	[-]	I	I	I	II	II	II	I	I	I	II	II	II

Table 3: *measured capacities and peak displacements*

As revealed by Table 3 only minor differences are observed within each of the four groups (S2, R2, S3 and R3) with respect to the resulting shear capacity, especially for the groups S2 and S3 provided with stirrups made from plain bars. For groups R2 and R3, provided with ribbed bars, a somewhat greater variation is observed. Also, when comparing groups S2 & R2 and S3 & R3, respectively, only minor differences are observed with respect to the shear capacity. Disregarding unintended variations of material parameters, all members within these corresponding groups (S2 & R2 and S3 & R3, respectively), was, as mentioned, expected to possess the same shear capacity, owing to the identities concerning the strength of the provided transverse reinforcement.

3.1.2 Load-displacement diagrams

In figures 4a and 4b load-displacement diagrams are shown for all tested members. The load refers to the shear force along the considered span, disregarding the presence of self-weight. The displacement refers to the downward displacement, measured using an LVDT located just next to the actuator, on the considered shear span. The diagrams are paired into two different groups, referring to the intended variation of the smeared tensile strength provided by the stirrups.

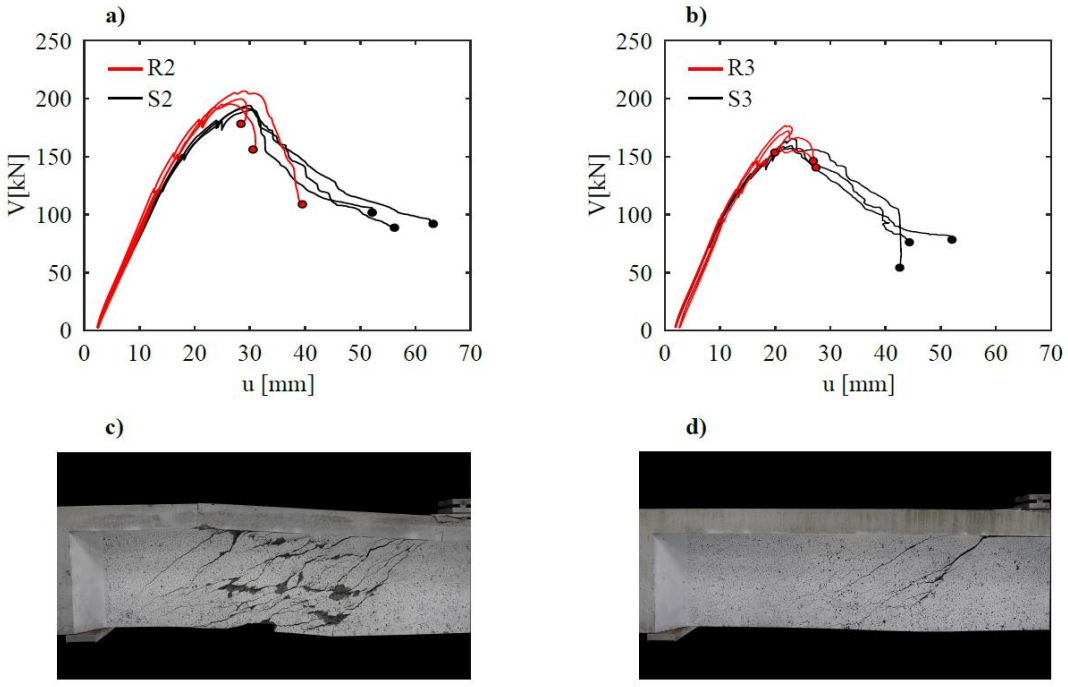

Figure 4: *load-displacement diagrams for* ***a)*** *groups S2 & R2* ***b)*** *groups S3 & R3.*

typical appearance for groups S and R after failure ***c)*** *S2a* ***d)*** *R2a*

As can be seen, an almost linear response is observed for all members in what could be regarded as the serviceability loading range. The differences regarding stirrup arrangement and their mechanical properties did not appear to materialize into noticeable differences concerning the overall stiffness for this range of loading. When approaching the peak load, the diagrams do seem to indicate a slightly greater degradation of stiffness in the case of members with stirrups made from plain or smooth bars (S2 and S3).

3.1.3 Failure modes

From an overall perspective the only consistent and substantial difference between the members was, as also revealed by the load-displacement diagrams, the mode of failure, and more specifically; the failure mechanism through which the shear failure evolved after reaching peak loading.

For the members with stirrups made from deformed bars (R2 and R3), the shear failure was violent and mostly very unstable. Even though loading was controlled through the rate of the piston-movement, the unloading process could not be controlled. It was confirmed from subsequent inspection that failure in all cases involved rupture of a number of stirrups, the distinct sound of which, in most cases, could be clearly heard during testing, in the second of collapse or just before.

On the contrary, all members with stirrups made from smooth bars (S2 and S3) failed in a rather stable manner, where the gradual softening, and corresponding unloading, could be easily controlled. The tests were stopped when the applied shear forces had been reduced to half of the peak load. However, the members were still able to carry the applied load at that point. Inspections revealed that no stirrups had ruptured in any of the members with plain stirrups.

In figures 4c and 4d pictures of members S2a and R2b are shown. The pictures refer to the situation just before the tests was stopped. Notice the pronounced differences regarding the damage induced during failure; In the case of beam S2a the collapse involved the gradual development of an extensive failure zone within the web along with significant local bending of the flange. This mode of failure was characteristic for the members with stirrups made from plain bars. On the contrary, the collapse of beam R2a involved a sudden extensive opening of one or two dominant cracks. The collapse was most likely triggered by rupture of the stirrups crossing these dominant cracks. The actual presence of such ruptured stirrups was, as mentioned, verified trough inspection after the tests had been stopped. This mode of failure, involving clearly visual localization of deformations, was characteristic for the members with stirrups made from ribbed bars.

3.2 Serviceability behaviour

3.2.1 Load range

In figures 5a-5d crack displacements and average web strains, belonging to the central region of the shear span are plotted against the applied load for one member from each of the four groups. As illustrated in the accompanying figure, the crack displacements refer to three different locations (top, mid and bottom) along the member depth whereas ε_y (dotted black curve) represents the average vertical web strain, measured using a squared grid (210·210 mm) centred at mid depth of the web.

The diagrams, which are practically identical for all the tested beams, reveal the presence of a reasonable linear range, lasting until a load of approximately $0.7 \cdot V_{u,test}$ is applied. In the following, the approximately linear range will be referred to as the serviceability range.

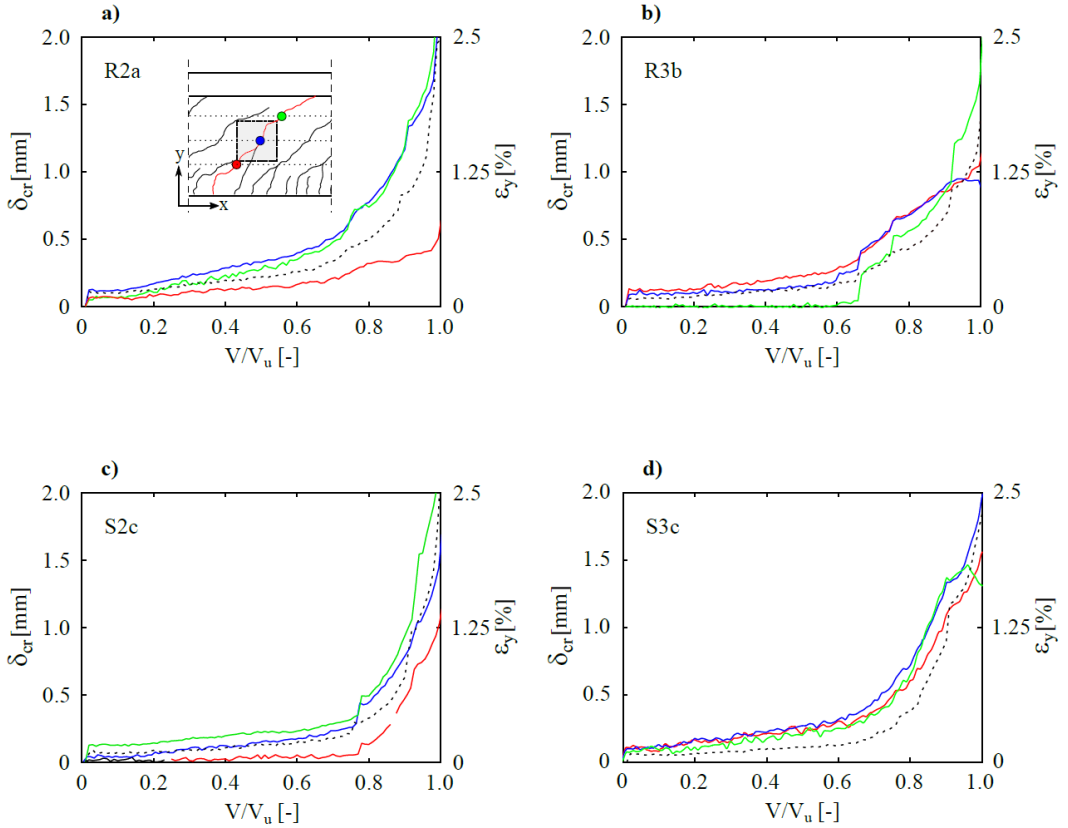

Figure 5: *crack displacements and average vertical web strain for selected beams.*

a) *R2a,* ***b),*** *R3b,* ***c)*** *S2c and* ***d)*** *S3c*

When considering cracks/measurements-grids located outside this central part of the shear span, the corresponding diagrams were found to remain linear for a greater loading range, indicating that yielding of stirrups was initiated in this central region. It is to be noticed, that the off-set at zero loading is due to crack displacements introduced during the first two load-cycles, leading to certain "residual" crack displacement at the beginning of the final loading cycle.

3.2.2 Crack pattern and crack displacements

Figures 6a-6d illustrates crack patterns, observed using the photogrammetric measurements, in members R2a, S2c, R3a and S3c at a load of approximately 60% of the peak load. The considered load step thus represents the final part of the serviceability range. Plots illustrating relative displacements within web cracks have been superimposed; only the most dominant cracks have been included in these measurements.

The observed cracks-patterns are well-known and somewhat characteristic for the considered type of members and can roughly be divided into two different groups of cracks; minor, mostly vertical, cracks at a small spacing in the region of the so-called tension chord, and a more coarse system of web cracks of more or less constant inclination. The observed patterns of web cracks in the serviceability range were, to a large extend, identical for all the tested members. Hence, the variations regarding bar surface profile and layout of the stirrup reinforcement did not appear to bring around any substantial differences what regards inclination and spacing of the cracks located in the web.

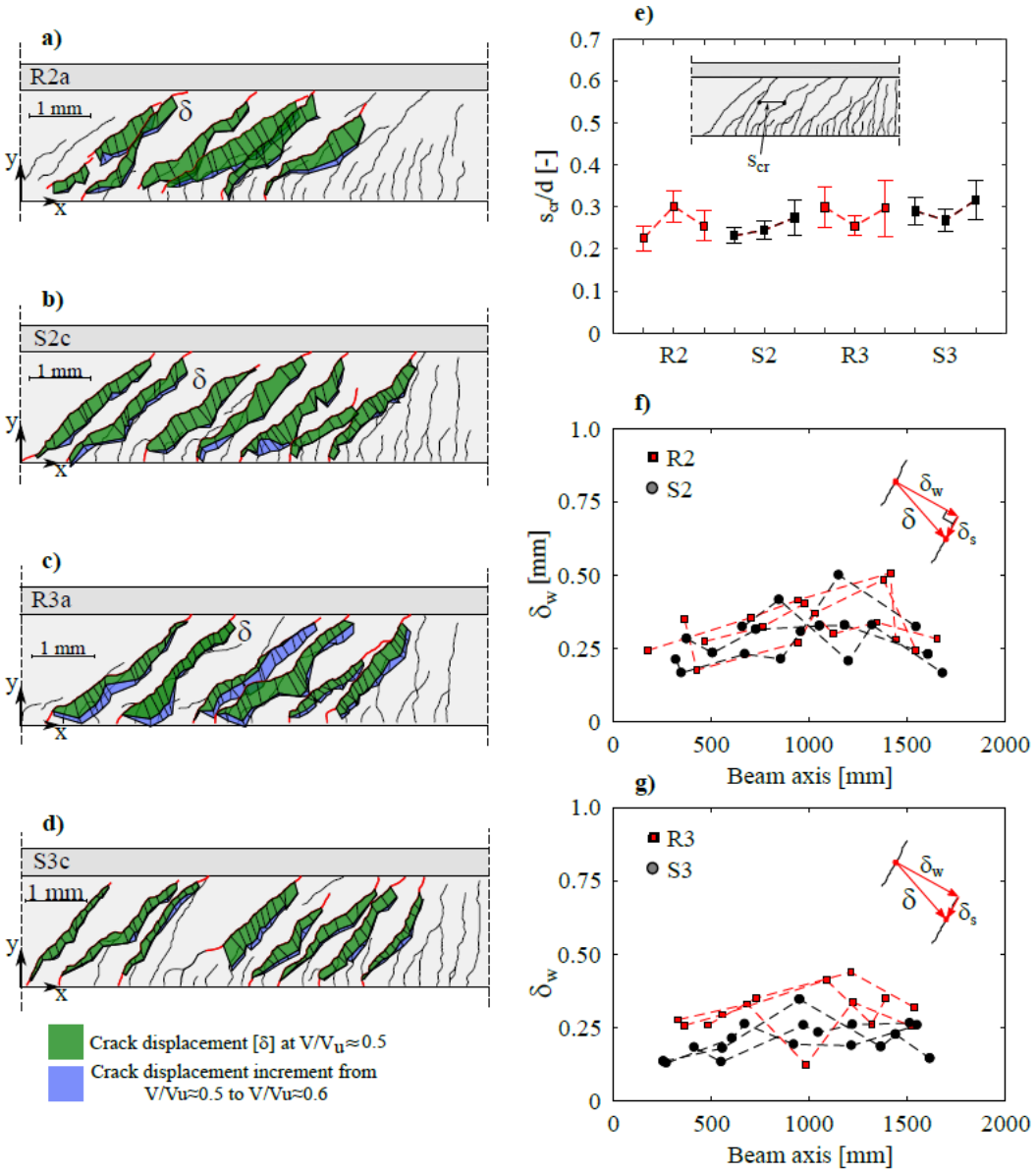

Figure 6: a)-d) *cracks and crack displacement at 0.6Vu,* ***e)*** *average web crack spacing.* ***f)-g)*** *maximum crack widths at 0.5Vu.*

The apparent similarities are further substantiated in figure 6e, where the average web crack spacing relatively to the effective height is plotted for all the members. Only cracks crossing mid height of the web have been included. A slight increase might be observed in regard to the average spacing as the amount of stirrups is lowered. However, the measurements are too scattered; especially for the members provided with stirrups made from deformed bars.

In regards to the relative crack displacements, the green shaded part represents the magnitude of the relative displacements taking place between zero load and approximately $0.5 \cdot V_{u,test}$, while the blue shaded part refers to the increment, when the load had been further increased to approximately $0.6 \cdot V_{u,test}$. Owing to the differences in shear capacity, and thus utilization of the concentrated longitudinal reinforcement, the crack displacements illustrated for R2a and S2c cannot be compared directly with those of R3a and S3c.

The plots reveal that the directions of relative crack displacements, except for a few local regions are largely perpendicular to the orientation of the corresponding cracks; in other words, the relative displacements are comprised of mainly crack opening, and apparently little sliding. Again, the variations regarding bar surface profile and layout of the stirrup reinforcement cannot be traced.

As might be expected, the crack displacements are generally somewhat greater around mid-depth of the members, when compared to the cracks in flexural tension chord. However, there seems to be no sizeable trend when considering the variation of the crack displacements across the height of the web. The magnitude of the web crack displacements appears not to be significantly influenced by the variation of the bending moment across the span, and thus the strain variation in the concentrated longitudinal reinforcement. This can also be observed in figure 6f and 6g, where maximum crack widths, δ_w, are plotted for all members. The measurements refer to dominating web cracks along the shear span, and only includes the maximum crack width for a given crack, wherever it may occur across the height of the given crack.

For all members, the crack width measurements relates to an applied load of approximately $0.5 \cdot V_{u,test}$, which in turn corresponds to a shear force of roughly 70% of the shear capacity predicted according to present provisions of the Eurocode, and using $\cot(\theta)=2.5$. The considered load level thus represents an upper limit of the service load in practical design. Again, the measurements seem to suggest that there is no sizeable influence from the stirrup design. However, if any, the measurements could indicate slightly smaller crack widths for the case of stirrups made from ribbed bars. Prior to testing it was the expectation of the authors that somewhat greater crack widths would, in fact, be experienced for members with plain stirrups. The improved bond of the ribbed bars was expected to bring around smaller crack spacings and smaller crack widths in the web.

3.3 Ultimate- and post-peak behaviour

3.3.1 Transition between load ranges

An applied load in the order $0.7 \cdot V_{u,test}$ marked the end of the serviceability range; irrespectively of the stirrup type and layout. For a further increase of the load, the tested beams all began to exhibit a non-linear and excessive increase with respect to the web crack displacements, as can be confirmed from figure 5. The pattern of web cracks, illustrated in figure 7a for the case of S3c, gradually changed and "flattened" with the emergence of new and more inclined web cracks, propagating in between and partly merging with the previously developed web cracks. Similar to what was observed during the "serviceability range", there appeared to be little or no systematic difference between the members in regard to this development. Additional crack patterns are illustrated in figures 10a-10d, showing the conditions close to and at peak-load. The horizontal cracks, running along the junction between web and flange, are not shown on these pictures.

3.3.2 Average strains

A strong indicator of the significant change of behaviour when approaching the peak-load, reflecting the likely redistribution of internal forces in the web, is shown in figure 7c. The diagram plots the measured relation between the applied load and the direction $\theta_{\varepsilon 2}$ of the minor principal strain in the central region of the shear span of beam S2c, determined using the aforementioned measurement-grid, illustrated in figure 7b, with the center located at mid height of the web. In the specific case, the angle of the minor principal strain direction decreases consistently from approximately 35° to 17° during the remaining load span, until peak was reached. Notice the almost constant rate at which the angle decreases.

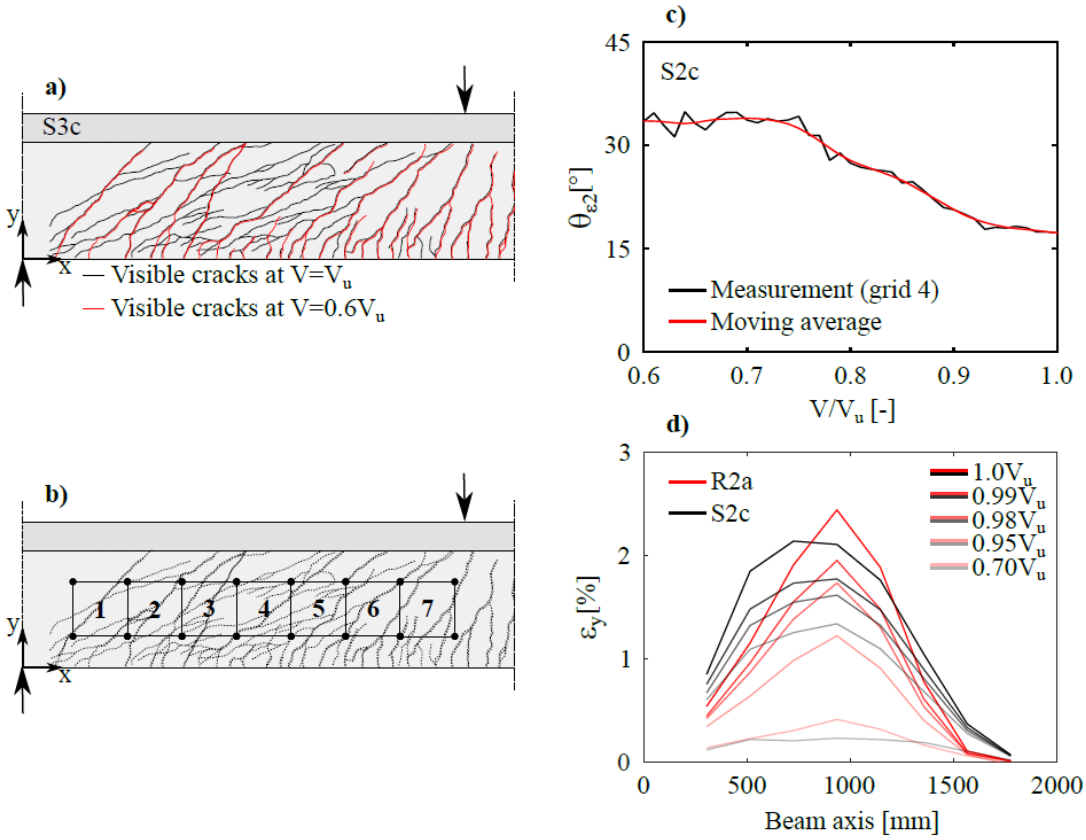

Figure 7: a) *change in crack pattern for S3c.* ***b)*** *measurement grid used for average strain calculations.*

c) *variation of minor principal strain direction for S2c.*

d) *variation of average vertical web strain across shear span for beams R2a and S2c.*

A similar behaviour was observed for all the tested beams. Average vertical strains ε_y within this central region have already been presented in figure 5, and by comparing the two diagrams, it can be seen that the re-orientation of the principal strains occurs simultaneously with an excessive increase of the crack displacements.

In figure 7d average vertical web strains ε_y and their variation along the beam axis are plotted for members R2a and S2c. The plots refers to load steps between $0.7 \cdot V_{u,test}$ and $V_{u,test}$. For both members the average strains are increased, more or less, by a factor of ten during the considered load span, revealing the introduction of significant plastic strains in the stirrups.

In figures 8a and 8b similar measurements of average vertical web strains at peak load are shown for all the beams. The plots reveal an almost identical behaviour when considering groups S2 and R2, while slightly more scattered results are obtained for groups S3 and R3. Based on these measurements there can, however, be no uncertainty that significant plastic strains in the stirrups must have developed over a large zone between the point of loading and support, with the maximum strains developed around the centre of the shear span.

The diagrams in figure 8a and 8b also includes measurements on the average horizontal web strain, ε_x, at peak load, estimated using the same square grid. For most members the maximum average strain is seen to occur close to the centre of the shear span, and not at the location of maximum bending moment. Despite the estimated flexural yield load not being reached, the average strain at mid height of the web in many cases still reaches a value equal to the yield strain of the flexural reinforcement. The significant strains at this level is due to the presence of large crack displacement at mid height of the web.

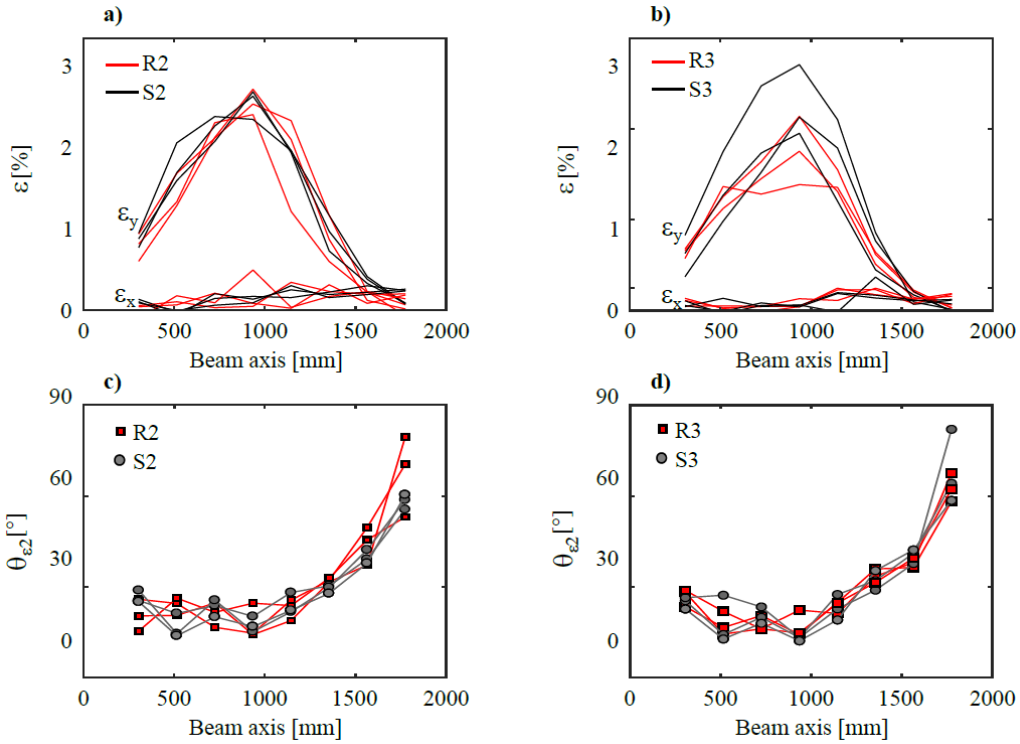

Figure 8: *variation of average web strains across shear span for groups* ***a)*** *R2 & S2* ***b)*** *R3 & S3. variation of minor principal strain direction across shear span for groups* ***c)*** *R2 & S2 and* ***d)*** *R3 & S3.*

Measurements on the minor principal strain direction $\theta_{\varepsilon 2}$ at peak load are presented in figures 8c and 8d for all the beams. The diagrams reveal a significant variation of the direction along the shear span, with the minimum value obtained approximately at mid span. The values in parentheses represents the mean of $\theta_{\varepsilon 2}$ of the fourth (central) measurement grid for each group of beams. According to these measurements there seem to be no apparent relation between the stirrup arrangement/type and the direction of the minor principal strain in general. Based upon visual comparison, the variation of $\theta_{\varepsilon 2}$ across the shear span appears to follow the same trend as the inclination of dominant web cracks present within the measurement-grid. When comparing specifically the apparent crack direction in the central part of the span with that of the minor principal strain in the central region (aforementioned mean values) the two quantities are found not to coincide, and the direction of $\theta_{\varepsilon 2}$ is consistently lower. For the sake of comparison, the inclination of a straight line running from the centre of the support to centre of load application is 16°.

3.3.3 Relative displacements

As revealed by the crack-patterns and web deformations presented so far, it is safe to conclude that a more or less identical behaviour was observed for all the beams until a load of approximately $0.90\text{-}0.95 \cdot V_{u,test}$ was reached. As previously mentioned, the post-peak behaviour and the mode of collapse was, in fact, the only significant difference between the members with stirrups made from plain bars (S2 and S3) and members with ribbed stirrups (R2 and R3).

In the case of the beams with ribbed stirrups, a tendency for the deformation of the web to be localized into only a few dominant web cracks could then be observed, and this tendency became gradually more pronounced close to and just beyond peak. In Figure 9 relative displacements are plotted for the most dominant web cracks in the case of beam R2a, representing one of the more marked cases of localization. The blue (90% to peak) -

and red (peak to collapse) shaded regions represent the incremental increase taking place between $0.9 \cdot V_{u,test}$ and collapse, where the relative displacements were observed to be almost fully localized within only two of multiple web cracks. Ultimately, this development led to the collapse, illustrated in figure 4d, for a deformation just slightly greater than the deformation at peak.

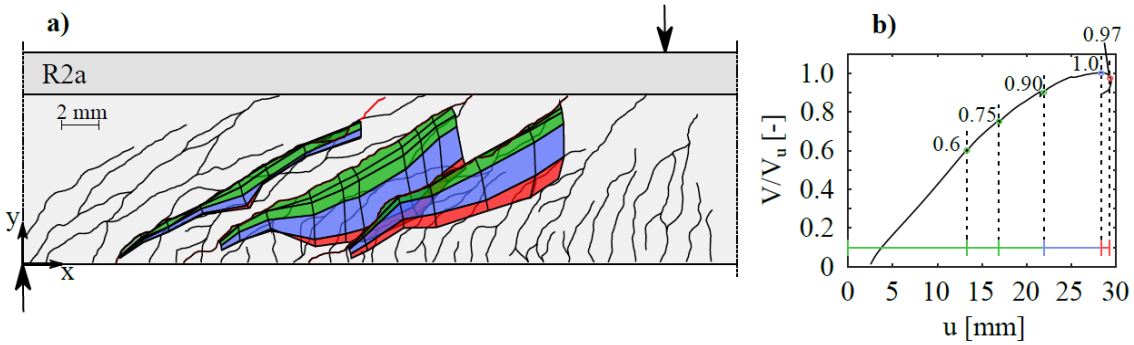

Figure 9: *crack displacements in dominating web cracks in beam R2a*

The plot also reveals the introduction of gradually increased crack slips. As mentioned earlier crack opening was found to be the dominant mode of crack displacement during the "SLS" load range, whereas the direction of the relative crack displacement at between peak and collapse are observed to be mainly downwards. To the extent that it could be investigated, this was observed for most of the tested beams, irrespective of the type of stirrups. However, owing to the extent of web cracking at peak - especially for the S-beams with smooth stirrups - it was not possible to carry out systematic DIC-measurements on the crack kinematics so close to collapse for all the beams, similar to those presented in figure 9.

In order to further study the deformations of the web, another approach was therefore taken, the result of which is illustrated in figures 10a to 10d. In the figures, the vertical component of the web-deformations along certain vertical lines is illustrated for one member from each of the four groups.

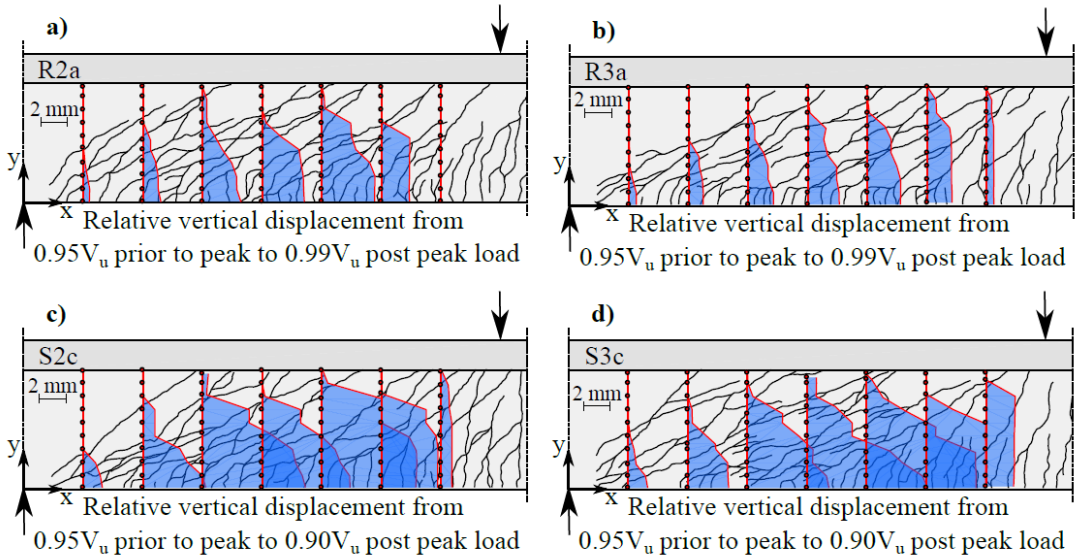

Figure 10: *relative vertical crack displacements around peak load for selected beams*

a) *R2a,* ***b)*** *R3a,* ***c)*** *S2c,* ***d)*** *S3c.*

The deformations are shown relatively to a line of reference aligned with the junction between web and flange, and are, furthermore, measured relatively to the deformations at $0.95 \cdot V_{u,test}$. Hence, only increments around peak are considered. In case of the R-beams (R2a and R3a) with deformed bars, the plots support the previously

mentioned tendency for the web deformations to be concentrated at the position of a few dominating inclined cracks. For the S-beams, the deformations are, first of all, seen to be much larger; also the deformations seems be more evenly distributed across the height of the web.

3.3.4 Flange deformations

The presentation of experimental observations will be concluded with a remark concerning the deformation of the flanges. As mentioned, the collapse of the members with smooth stirrups involved significant local bending deformation of the flanges. As is visible in figure 4c, the deformations where localized into discrete "hinges". The locations of these hinges could easily be visually determined owing to the significant localized flexural cracking at the location of the flange slope-discontinuities. As can be seen from this picture the "failure zone" in the web takes the appearance of an inclined band, bounded by parallel inclined lines, and extending almost across the entire span. The "hinges" are located at the intersection between the bounding lines and the flange.

However, such significant deformations where only introduced during the post-peak failure process. Based on LVDT-measurements of the vertical displacements along the flange, slope-discontinuities, in general, could not be observed before the downward deformation at the point of loading had reached 1.4-1.5 of the deformation at peak load. As can be seen on the load-displacement diagrams, the applied load had thus dropped significantly at this point.

Similar mobilization of the flange was in general not observed in the case of the beams with deformed stirrups, due to prior rupture of the stirrups and thereby collapse of the beams.

4 Conclusions

The focus of the presented investigation was to study the influence of the transverse reinforcement type and layout on the cracking- and deformational behaviour and shear capacity of thin-webbed reinforced concrete T-beams subjected to shear and bending. Specifically, the results of twelve tests involving stirrups made from deformed and plain bars, respectively, and variable stirrups spacings have been presented and analysed. On this basis, the following conclusions are made:

- The considered type and arrangement of stirrups within groups of comparable equivalent tensile strength $f_{t,s}$ did not appear to be of influence in regards to the spacing and orientation of web-cracks and the kinematics of these cracks under service load conditions. Maximum crack widths were found to be of similar magnitude.

- Increasing the amount of transverse reinforcement led to an expected increase of the shear capacity. The investigated type and arrangement of stirrups within groups of comparable equivalent tensile strength did not appear to be of influence regarding the observed shear capacity.

- The considered type and arrangement of stirrups within groups of comparable equivalent tensile strength had no apparent influence what regards the deformations of the web prior to peak.

- A pronounced difference regarding mode of failure was observed. In contrast to the predominantly brittle failures observed in members with deformed stirrups, the beams with plain transverse bars failed due to gradual softening of the web concrete. Under the prerequisite of sufficient strain capacity of the stirrups, the presence of the flange is likely to be of fundamental influence for this mode of failure, and the development of the failure zone in the web.

Literature

[1] Timoshenko, S. P., J. M. Gere. Theory of Elastic Stability. Chapter 8 and 9. Second edition. Dover Publications, Inc.
[2] Nielsen, M. P. and Hoang, L. C. Limit Analysis and Concrete Plasticity. CRC Press, 3rd edition. 2010.
[3] Eurocode 2 . Design of concrete structures - Part 1-1: General rules and rules for buildings. European Committee for Standardization Eurocod

Danish Society for Structural Science and Engineering

Requests for membership of the society are submitted to one of the board members:

Kåre Flindt Jørgensen, Chairman of the Board
NCC Danmark. Mail: karjor@ncc.dk

Andreas Bollerslev, Vice Chair
Niras. Mail: anbo@niras.dk

Kirsten Riis, Secretary
Vejdirektoratet. Mail: kiri@vd.dk

Mikkel Christiansen, Cashier
AB Clausen. Mail: dsby.mc@gmail.com

Gunnar Ove Bardtrum, Board member
BaneDanmark. Mail: goba@bane.dk

Jesper Pihl, Board member
Cowi. Mail: jepi@cowi.dk

Dennis Cornelius Pedersen, Board member
MOE. Mail: dcpe@moe.dk

Jens Henrik Nielsen, Board member
DTU. Mail: jhn@byg.dtu

The purpose of the society is to work for the scientific development of structural mechanics - both theory and construction of all kinds of load-bearing structures - promote interest in the subject, work for a collegial relationship between its practitioners and assert its importance to and in collaboration with other branches of engineering. The purpose is sought realized through meetings with lectures and discussions as well as through the publication of the Proceedings of the Danish Society for Structural Science and Engineering.

Individual members, companies and institutions that are particularly interested in structural mechanics or whose company falls within the field of structural mechanics can be admitted as members.